Int. J. Solids Structures Vol. 23, No. 12, pp. 1679–1698, 1987
Printed in Great Britain.

0020-7683/87 $3.00+ .00

BOUNDARY ELEMENT ANALYSIS OF INELASTIC AXISYMMETRIC PROBLEMS WITH LARGE STRAINS AND ROTATIONS

HARINDRA RAJIYAH and SUBRATA MUKHERJEE
Department of Theoretical and Applied Mechanics, Kimball Hall, Cornell University, Ithaca, NY 14853, U.S.A.

(*Received* 12 *December* 1986; *in revised form* 1 *May* 1987)

Abstract—The subject of this paper is a boundary element method (BEM) formulation and numerical implementation for inelastic axisymmetric problems in the presence of small elastic strains but large inelastic strains and rotations. A rate formulation with an elastic–viscoplastic material model, together with an updated Lagrangian description of the problem, is used in this paper. Careful attention is paid here to the analytical and numerical treatment of the complicated and sensitive kernels that arise in these integral equations for axisymmetric problems. A BEM computer program has been developed for the solution of general large strain–large rotation inelastic axisymmetric boundary/initial value problems. Numerical results for some sample problems are obtained from the BEM computer program and these results are compared against direct solutions.

INTRODUCTION

The subject of this paper is the analysis of axisymmetric problems in solid mechanics in the presence of small elastic strains but large inelastic strains and rotations. Such a situation commonly exists during the forming of metals. A rate formulation, together with an updated Lagrangian description of the problem, is used in this paper. The method of analysis is the boundary element method (BEM).

Mukherjee and his co-authors have considerable experience in the solution of elastic–viscoplastic problems by the boundary element method. Their research, up to 1982, is summarized in a book by Mukherjee[1]. Small strain planar and axisymmetric problems, together with other problems such as torsion, plate bending and inelastic fracture, are discussed in this book. During the past few years, Mukherjee and Chandra[2–4] have proposed a BEM formulation for elastic–viscoplastic materials subjected to large inelastic strains and rotations, and have applied this formulation to the study of sheet metal forming[5] and metal extrusion[6]. The numerical applications of the BEM, presented in Refs [2–6], have been limited to two-dimensional (plane strain or plane stress) problems.

Metal forming applications under axisymmetric conditions—such as the bulging of circular plates, drawing of tubes or extrusion of bars of circular cross-section, are far more common than those under planar conditions. As described carefully by Sarihan and Mukherjee[1, 7] among others, the modelling of axisymmetric problems by the BEM is far more challenging than its planar counterpart. The primary reason for this is that the kernels in the integral equations of the axisymmetric BEM formulation contain elliptic functions. These kernels are singular and sensitive and, in general, cannot be integrated in closed form even over boundary elements or internal cells of simple shape. Thus, special methods must be developed for the accurate numerical integration of these kernels over discrete elements. Typically, this requires the use of suitable analytical techniques before numerical quadrature can be employed.

The axisymmetric elastic BEM problem first received attention from Kermanidis[8] and Cruse *et al.*[9], followed by others such as Shippy *et al.*[10]. The small strain–small rotation axisymmetric elastic–plastic problem has been attempted, among others, by Cathie and Banerjee[11], Telles[12] and Sarihan and Mukherjee[7]. The work of Sarihan and Mukherjee[7] carefully describes the difficulties of boundary and domain integration of the axisymmetric kernels and suggests methods for overcoming these problems. Comparisons of BEM, finite element method (FEM) as well as direct solutions (whenever possible) are available in Ref. [7] for several illustrative problems.

Turning now to problems including both material and geometrical nonlinearities, the work of Mukherjee and Chandra[2–6] still appears to be the only study of its kind that uses the BEM as the method of choice for this class of problems. These papers present the general three-dimensional integral equations for these problems based on a rate formulation and an updated Lagrangian description. A detailed discussion of the derivation of these equations appears in a review article by Mukherjee and Chandra[4]. Numerical implementation of these equations, however, have been so far limited to planar problems.

This paper presents an analysis of axisymmetric problems in the presence of material as well as geometrical nonlinearities. The governing integral equations for this problem are first derived from the corresponding three-dimensional ones. The case of the solid body, where source points must be allowed to lie on the axis of rotation, is addressed as well. Next, similar equations are derived for the boundary traction rates and internal strain rates. The latter quantities are determined pointwise by analytical differentiation of the velocity equation at an internal point. Such an approach preserves one of the key advantages to the BEM in that jumps in stresses, caused by the numerical modelling in a method such as the FEM, are completely eliminated throughout the interior of the body.

Derivation of the integral equations governing internal strain rates is tricky in that kernels that are already $1/r$ singular (r being the distance between a source and a field point) must be differentiated at an internal source point. This is carried out in this paper following the method outlined by Bui[13] and the free terms arising out of all the integrals are given here. This still leaves the problem of numerical evaluation of the principal values of integrals which are $1/r^2$ singular. A new method for accurate numerical evaluation of these integrals, involving the use of the symbolic computer package MACSYMA[14], is presented here. It is expected that this approach will prove to be very powerful whenever integrals with such strong singularities must be evaluated numerically.

Numerical results for certain selected illustrative problems are presented at the end of this paper. The inelastic constitutive model due to Anand[15] is used here to describe material behavior. The computer program is flexible with regard to choice of a viscoplastic material model and the one used here is for illustrative purposes only. The results from the BEM analysis are compared with direct solutions.

GOVERNING EQUATIONS

Integral equations for 3-D problems

Following earlier publications by Mukherjee and Chandra[2–6], the velocity $\mathbf{v}$ at an internal source point p, in a solid subjected to (three-dimensional) small elastic strains but large inelastic strains and rotations, can be written as $(i,j,k,l,m = 1,2,3)$

$$v_j(p) = \int_{\partial B^0} [U_{ij}(p,Q)\dot{t}_i(Q) - T_{ij}(p,Q)v_i(Q)]\, \mathrm{d}S_Q^0 + \int_{B^0} [2GU_{ij,k}(p,q)d_{ik}^{(n)}(q)]\, \mathrm{d}V_q^0 + \int_{B^0} [U_{ij,m}(p,q)G_{mikl}(q)v_{k,l}(q)\, \mathrm{d}V_q^0 \quad (1)$$

where U_{ij} and T_{ij} are the usual kernels for infinitesimal isotropic elasticity that are available in many references (e.g. Ref. [1]) and p and q are source and field points, respectively (with capital letters denoting points on the reference boundary ∂B^0 and lower case letters denoting points inside the body with reference configuration B^0), and a comma denotes differentiation with respect to a field point. Further, the Lagrangian traction rates are denoted as $\dot{t}_i$, the tensor G_{ijkl}, in terms of the components of the Cauchy stress σ_{ij} and the Kronecker delta δ_{ij}, is

$$2G_{ijkl} = \sigma_{ik}\delta_{jl} + \sigma_{jl}\delta_{ik} + \sigma_{jk}\delta_{li} - \sigma_{li}\delta_{jk} \quad (2)$$

and $d_{ij}^{(n)}$ is the non-elastic part of the symmetric velocity gradient, i.e.

$$d_{ij} = d_{ij}^{(e)} + d_{ij}^{(n)} = \frac{1}{2}\left[\frac{\partial v_i}{\partial x_j} + \frac{\partial v_j}{\partial x_i}\right]. \tag{3}$$

Material coordinates in the reference configuration are called X_i and in the current configuration x_i. As mentioned before, an updated Lagrangian formulation is used here so that, within each time step, the deformation gradient $\mathbf{F} \approx \mathbf{I}$ and $\mathbf{x} \approx \mathbf{X}$.

It is useful to mention here that the spin ω is taken as

$$\omega_{ij} = \frac{1}{2}\left[\frac{\partial v_i}{\partial x_j} - \frac{\partial v_j}{\partial x_i}\right] \tag{4}$$

and a hypoelastic model is assumed in which the Jaumann rate of the Cauchy stress, $\mathring{\sigma}_{ij}$, is related to the elastic part of the symmetric velocity gradient as

$$\mathring{\sigma}_{ij} = \lambda d_{kk}^{(e)}\delta_{ij} + 2G d_{ij}^{(e)} \tag{5}$$

where λ and G are the usual Lamé parameters. The non-elastic rates $d_{ij}^{(n)}$ must be obtained from an appropriate material constitutive model.

Other important assumptions that have been used to derive eqn (1) are that the non-elastic portion of the symmetric velocity gradient is volume preserving, i.e.

$$d_{kk}^{(n)} = 0 \tag{6}$$

and also that the total deformation, which becomes mostly nonelastic as the deformation proceeds, is also nearly incompressible so that the Jaumann rate of the Kirchhoff stress $\mathring{\tau}$ is assumed to equal that of the Cauchy stress $\mathring{\sigma}$. Finally, physical body forces are also assumed to be absent in this analysis. Each of these assumptions can be easily relaxed and the full equations are given in Ref. [4].

Physically, eqn (1) relates the velocity at an internal point in the deforming solid to the velocity and traction rates on the boundary as well as to velocity gradients inside the body. The first surface integral on the right-hand side of eqn (1) is the usual one for linear elasticity (except for the interpretation of $\dot{\tau}$ which follows), and the first domain integral is analogous to the one in small strain–small rotation inelastic BEM analysis[1, 16]. The last domain integral arises due to finite strains and rotations inside the body and is sometimes called the "geometric correction" in the finite element literature.

The boundary of the body, of course, undergoes large strains and normals to the boundary experience large rotations during deformation. Thus, the so-called "load correction" effect, is reflected in the equation

$$\dot{\tau}_i = n_j \dot{s}_{ji} = \dot{t}_i - n_j G_{jikl} v_{k,l} \tag{7}$$

which relates the Lagrange traction rate $\dot{\tau}_i$ (s_{ji} are the components of the non-symmetric nominal or Lagrange stress) to the "usual" traction rate $\dot{t}_i$

$$\dot{t}_i = n_j \mathring{\sigma}_{ji}. \tag{8}$$

The rate $\dot{t}_i$ can be interpreted as a component of the rate of the prescribed follower force, per unit deformed surface area, on the deforming boundary. It is important to note that eqn (7) introduces the unknown velocity gradients also on the boundary of the body.

The corresponding boundary integral equation can be obtained from eqn (1) in the usual way by taking the limit as $p \to P$. This replaces $v_j(p)$, on the left-hand side of eqn (1), by $C_{ij}(P)v_j(P)$ (where $\mathbf{C}$ is the well-known corner tensor) and p by P in every term on its right-hand side[2–6].

Velocity gradients at an internal point are best obtained by analytical differentiation of eqn (1) at a source point p. A differentiated version of eqn (1) is obtained as

$$v_{j,I}(p) = \int_{\partial B^0} [U_{ij,I}(p,Q)\dot{t}_i(Q) - \dot{T}_{ij,I}(p,Q)v_i(Q)]\,\mathrm{d}S_Q^0 + \frac{\partial}{\partial x_I}\int_{B^0} 2GU_{ij,k}(p,q)d_{ik}^{(n)}(q)\,\mathrm{d}V_q^0 + \frac{\partial}{\partial x_I}\int_{B^0} U_{ij,m}(p,q)G_{mikn}(q)v_{k,n}(q)\,\mathrm{d}V_q^0 \quad (9)$$

where I denotes differentiation at a source point.

Differentiation of the domain integrals must be carried out with great care since the kernels $U_{ij,k}$ are already $1/r^2$ singular for 3-D problems. Details of carrying out this procedure are given later in this paper in the context of axisymmetric problems.

Once the velocity gradients are determined inside the body by iterative solution of the appropriate equations, it is a simple matter to determine d_{ij}, then $d_{ij}^{(e)}$ from eqn (3), the Jaumann rates of the Cauchy stress from eqn (5) and finally the material rates of the Cauchy stress.

The stress rates on the boundary of the body are best determined by using a different algorithm rather than by taking the limit of eqn (9) as $p \to P$[1]. This matter will be taken up again later in the context of axisymmetric problems.

Integral equations for axisymmetric problems

An axisymmetric body with axisymmetric loading is considered in this paper. Using cylindrical polar coordinates R, θ and Z, the non-zero components of displacements, stresses and strains are u_R, u_Z, ε_{RR}, $\varepsilon_{\theta\theta}$, ε_{ZZ}, $\varepsilon_{RZ}(=\varepsilon_{ZR})$, σ_{RR}, $\sigma_{\theta\theta}$, σ_{ZZ} and σ_{RZ} $(=\sigma_{ZR})$. All dependent variables are functions of R, Z, and t. Some torsion problems can be independent of θ but these are not considered in this formulation.

The notation used here is the same as in Refs [1, 7] and is shown in Fig. 1. The source point is denoted by (R, O, Z) and the field point by (ρ, θ, ζ). Since the problem is axisymmetric, it is sufficient to choose the source point in the x_1–x_3 plane.

The axisymmetric BEM equations are derived from eqn (1) by integrating the kernels U_{ij}, T_{ij}, etc. for the field point moving around a ring keeping the source point fixed.

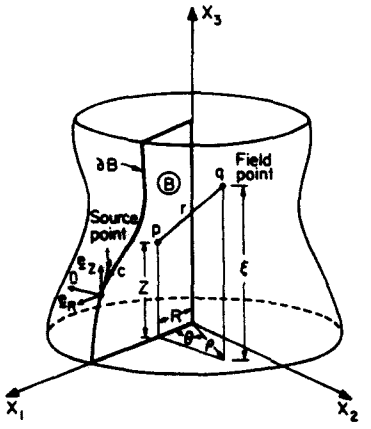

Fig. 1. Geometry of the axisymmetric problem.

Integrating θ from 0 to 2π in eqn (1) results in ($j = 1$ and 3, no sum over ρ or ζ)

$$
\begin{aligned}
v_j = & \int_{\partial B^0} [U_{\rho j}\dot{\tau}_\rho + U_{\zeta j}\dot{\tau}_\zeta - T_{\rho j}\dot{u}_\rho - T_{\zeta j}\dot{u}_\zeta]\rho_0 \, \mathrm{d}c_0 \\
& + 2G \int_{B^0} \left[U_{\rho j,\rho} d^{(n)}_{\rho\rho} + U_{\rho j,\zeta} d^{(n)}_{\rho\zeta} + U_{\zeta j,\rho} d^{(n)}_{\zeta\rho} \right. \\
& \left. + U_{\zeta j,\zeta} d^{(n)}_{\zeta\zeta} + \frac{U_{\rho j} d^{(n)}_{\theta\theta}}{\rho_0} \right] \rho_0 \, \mathrm{d}\rho_0 \, \mathrm{d}\zeta_0 + \int_{B^0} \left[U_{\rho j,\rho} [\sigma_{\rho\rho} d_{\rho\rho} + \sigma_{\rho\zeta}(d_{\rho\zeta} + \omega_{\rho\zeta})] \right. \\
& + U_{\rho j,\zeta} [\sigma_{\rho\rho} d_{\rho\zeta} + \sigma_{\rho\zeta} d_{\zeta\zeta} + \sigma_{\zeta\zeta}\omega_{\rho\zeta}] + U_{\zeta j,\rho} [-\sigma_{\rho\rho}\omega_{\rho\zeta} + \sigma_{\rho\zeta} d_{\rho\rho} + \sigma_{\zeta\zeta} d_{\rho\zeta}] \\
& \left. + U_{\zeta j,\zeta} [\sigma_{\rho\zeta}(d_{\rho\zeta} - \omega_{\rho\zeta}) + \sigma_{\zeta\zeta} d_{\zeta\zeta}] + \frac{U_{\rho j}\sigma_{\theta\theta} d_{\theta\theta}}{\rho_0} \right] \rho_0 \, \mathrm{d}\rho_0 \, \mathrm{d}\zeta_0
\end{aligned} \tag{10}
$$

where, because of axisymmetry, $\dot{u}_R = \dot{u}_1$, $\dot{u}_Z = \dot{u}_3$ and $\mathrm{d}c_0 = \sqrt{(\mathrm{d}\rho^2 + \mathrm{d}\zeta^2)}$ is an element on the boundary of the ρ–ζ plane. The domain B^0 and boundary ∂B^0 in the above equation now refer to a generator plane of the axisymmetric solid and its boundary (excluding the portion on the x_3-axis), respectively (Fig. 1), so that the three-dimensional problem is effectively reduced to a two-dimensional one. Also, eqn (9) is valid for the velocity at an internal source point. The corresponding boundary integral equation is obtained, as usual, by taking the limit $p \to P$ which introduces the corner tensor C_{ij}[1, 7].

The kernels for the case $p \notin$ the axis of symmetry are given in Refs [1, 7] (the kernels $U_{\zeta 1}$ and $U_{\rho 3}$ had been inadvertently transposed in these references). If $p \in$ the axis of symmetry, as must be considered for solid bodies without axial holes in them, one gets

$$
\begin{aligned}
U_{\rho 1} &= 0, \qquad U_{\rho 3} = \frac{(\zeta - Z)\rho}{8(1-\nu)Gr^3} \\
U_{\zeta 1} &= 0, \qquad U_{\zeta 3} = \frac{1}{8(1-\nu)G} \left[\frac{(3-4\nu)}{r} + \frac{(\xi - Z)^2}{r^3} \right]
\end{aligned} \tag{11}
$$

where ν is the Poisson's ratio of the material. It is interesting to note that the non-zero kernels above are $1/r$ (rather than $\ln r$) singular.

The traction kernels $T_{\rho j}$ and $T_{\zeta j}$ are linear combinations of $U_{\rho j}$ and derivatives of $U_{\rho j}$ and $U_{\zeta j}$ with respect to ρ and ζ[1, 7]. The explicit forms of the differentiated kernels $U_{\rho j,\rho}$, etc. for the case $p \notin$ axis of symmetry, are given in Ref. [17]. For the case $p \in$ axis of symmetry, one gets the relatively simple forms

$$
\begin{aligned}
T_{\rho 1} &= 0, \quad T_{\rho 3} = -\frac{1}{4(1-\nu)r^2} \left[\frac{3\rho(\zeta - Z)}{r^2} \frac{\partial r}{\partial n} + (1-2\nu) \left\{ \frac{\rho n_\zeta}{r} - \frac{(\zeta - Z)}{r} n_\rho \right\} \right] \\
T_{\zeta 1} &= 0, \quad T_{\zeta 3} = -\frac{\partial r/\partial n}{4(1-\nu)r^2} \left[(1-2\nu) + \frac{3(\zeta - Z)^2}{r^2} \right]
\end{aligned} \tag{12}
$$

where

$$
\frac{\partial r}{\partial n} = \frac{(\zeta - Z)}{r} n_\zeta + \frac{\rho n_\rho}{r}.
$$

It is interesting to note that even though, for example, $U_{\rho 1} = 0$ in eqn (11), kernels like $U_{\rho 1,\rho}$ for $p \in$ axis of symmetry are nonzero. These are determined by considering the appropriate components of the 3-D $U_{ij,k}$ kernel, setting $R = 0$ and then integrating θ from 0 to 2π.

The Lagrangian traction rates from eqn (7) become

$$\dot{\tau}_\rho = \dot{t}_\rho - n_\rho[\sigma_{\rho\rho}d_{\rho\rho} + \sigma_{\rho\zeta}(d_{\rho\zeta} + \omega_{\rho\zeta})] - n_\zeta[\sigma_{\rho\rho}d_{\rho\zeta} + \sigma_{\rho\zeta}d_{\zeta\zeta} + \sigma_{\zeta\zeta}\omega_{\rho\zeta}]$$
$$\dot{\tau}_\zeta = \dot{t}_\zeta - n_\rho[-\sigma_{\rho\rho}\omega_{\rho\zeta} + \sigma_{\rho\zeta}d_{\rho\rho} + \sigma_{\zeta\zeta}d_{\rho\zeta}] - n_\zeta[\sigma_{\rho\zeta}(d_{\rho\zeta} - \omega_{\rho\zeta}) + \sigma_{\zeta\zeta}d_{\zeta\zeta})]. \tag{13}$$

Velocity gradients at an internal point are obtained, as usual, by differentiating eqn (10) at internal source point p. Referring to eqn (10), the term on the left-hand side becomes $v_{j,I}$ and the boundary integral on the right-hand side becomes

$$\int_{\partial B^0} [U_{\rho j,I}\dot{\tau}_\rho + U_{\zeta j,I}\dot{\tau}_\zeta - T_{\rho j,I}\dot{u}_\rho - T_{\zeta j,I}\dot{u}_\zeta]\rho_0 \, dc_0.$$

The derivatives can be immediately moved under the integral sign in the above expression since p is an internal point, Q is a boundary point and the above integral is regular. Such, however, is not the case for the domain integrals in eqn (10), which are, in general, $1/r$ singular.

The derivatives $\partial I/\partial x_I$, where I is either of the domain integrals on the right-hand side of eqn (10), can be evaluated using the method outlined by Bui[13]. Free terms result from this process. The appropriate free terms from the various derivatives of the displacement kernels, for the cases $p \notin$ on the axis of symmetry and $p \in$ on the axis of symmetry, are listed in Tables 1 and 2, respectively. It is very interesting to note from Table 2 that free terms result from some first derivatives of $U_{\rho 1}$ and $U_{\rho 3}$ if $p \in$ on the axis of symmetry.

The actual free terms in an equation for $v_{j,I}$ are obtained by multiplying the appropriate terms in Table 1 or 2 with the corresponding terms from eqn (10). Thus, for example, the explicit form of the equation for $v_{1,1}$ is (no sum over ρ or ζ, $p \notin x_3$-axis)

$$\begin{aligned}
v_{1,1} = & \int_{\partial B^0} [U_{\rho 1,1}\dot{\tau}_\rho + U_{\zeta 1,1}\dot{\tau}_\zeta - T_{\rho 1,1}\dot{u}_\rho - T_{\zeta 1,1}\dot{u}_\zeta]\rho_0 \, dc_0 \\
& + 2G \int_{B^0 - B^0_\eta(p)} \Bigg[U_{\rho 1,\rho 1}d^{(n)}_{\rho\rho} + U_{\rho 1,\zeta 1}d^{(n)}_{\rho\zeta} + U_{\zeta 1,\rho 1}d^{(n)}_{\zeta\rho} \\
& + U_{\zeta 1,\zeta 1}d^{(n)}_{\zeta\zeta} + U_{\rho 1,1}\frac{d^{(n)}_{\theta\theta}}{\rho_0}\Bigg]\rho_0 \, d\rho_0 \, d\zeta_0 + \frac{5-8\nu}{8(1-\nu)}d^{(n)}_{\rho\rho}(p) - \frac{1}{8(1-\nu)}d^{(n)}_{\zeta\zeta}(p) \\
& + \int_{B^0 - B^0_\eta(p)} \Bigg[U_{\rho 1,\rho 1}[\sigma_{\rho\rho}d_{\rho\rho} + \sigma_{\rho\zeta}(d_{\rho\zeta} + \omega_{\rho\zeta})] \\
& + U_{\rho 1,\zeta 1}[\sigma_{\rho\rho}d_{\rho\zeta} + \sigma_{\rho\zeta}d_{\zeta\zeta} + \sigma_{\zeta\zeta}\omega_{\rho\zeta}] + U_{\zeta 1,\rho 1}[-\sigma_{\rho\rho}\omega_{\rho\zeta} + \sigma_{\rho\zeta}d_{\rho\rho} + \sigma_{\zeta\zeta}d_{\rho\zeta}] \\
& + U_{\zeta 1,\zeta 1}[\sigma_{\rho\zeta}(d_{\rho\zeta} - \omega_{\rho\zeta}) + \sigma_{\zeta\zeta}d_{\zeta\zeta}] + \frac{U_{\rho 1,1}\sigma_{\theta\theta}d_{\theta\theta}}{\rho_0}\Bigg]\rho_0 \, dr_0 \, d\zeta_0 \\
& + \frac{5-8\nu}{16G(1-\nu)}[\sigma_{\rho\rho}(p)d_{\rho\rho}(p) + \sigma_{\rho\zeta}(p)(d_{\rho\zeta}(p) + \omega_{\rho\zeta}(p))] \\
& - \frac{1}{16G(1-\nu)}[\sigma_{\rho\zeta}(p)(d_{\rho\zeta}(p) - \omega_{\rho\zeta}(p)) + \sigma_{\zeta\zeta}(p)d_{\zeta\zeta}(p)]
\end{aligned} \tag{14}$$

where $B^0_\eta(p)$ is a circle of small radius η, centered at p, in the plane of the generator of the axisymmetric solid. The Cauchy principal values of these integrals, with $\eta \to 0$, must be accurately evaluated numerically in a successful numerical implementation of this problem. This is, in general, a formidable task since the integrands are $1/r^2$ singular. A new, accurate analytical/numerical technique for carrying out this task is described in the section called "numerical implementation" later in the paper. The explicit forms of the kernels $U_{ij,kl}$ are given in Rajiyah's Ph.D. thesis[18]. As mentioned before, it is a simple matter to obtain the

Table 1. Free terms in the velocity gradient equations for the case $p \notin$ the axis of symmetry

Kernel	Free term from radial differentiation ($\bar{I} = 1$)	Free terms from axial differentiation ($\bar{I} = 3$)
$U_{\rho 1,\rho}$	$\frac{5-8\nu}{16(1-\nu)G}$	0
$U_{\rho 1,\zeta}$	0	$\frac{7-8\nu}{16(1-\nu)G}$
$U_{\zeta 1,\rho}$	0	$-\frac{1}{16(1-\nu)G}$
$U_{\zeta 1,\zeta}$	$-\frac{1}{16(1-\nu)G}$	0
$U_{\rho 3,\rho}$	0	$-\frac{1}{16(1-\nu)G}$
$U_{\rho 3,\zeta}$	$-\frac{1}{16(1-\nu)G}$	0
$U_{\zeta 3,\rho}$	$\frac{7-8\nu}{16(1-\nu)G}$	0
$U_{\zeta 3,\zeta}$	0	$\frac{5-8\nu}{16(1-\nu)G}$

Jaumann and then the material rates of the Cauchy stress at an internal point once the velocity gradients have been determined at that point. For this purpose, it is useful to record the relationship between the material and Jaumann rates of components of the Cauchy stress in cylindrical polar coordinates. These equations take the form

$$\begin{aligned}
\mathring{\sigma}_{RR} &= \dot{\sigma}_{RR} - 2\sigma_{RZ}\omega_{RZ} \\
\mathring{\sigma}_{\theta\theta} &= \dot{\sigma}_{\theta\theta} \\
\mathring{\sigma}_{RZ} &= \dot{\sigma}_{RZ} + \sigma_{RR}\omega_{RZ} - \sigma_{ZZ}\omega_{RZ} \\
\mathring{\sigma}_{ZZ} &= \dot{\sigma}_{ZZ} + 2\sigma_{RZ}\omega_{RZ}.
\end{aligned} \tag{15}$$

The boundary stress rates, at any time, are best obtained from a boundary algorithm rather than by trying to take the limit of an equation like eqn (14) as $p \to P$. This approach, which requires tangential differentiation of the displacement (or velocity in a rate formulation) components at a boundary point, was first suggested for linear elastic problems by Rizzo and Shippy[19]. This idea has been generalized to non-elastic problems with small strains and rotations by Sarihan and Mukherjee[1, 7].

Table 2. Non-zero free terms in the velocity gradient equations for the case $p \in$ the axis of symmetry

Kernel	Free terms from radial differentiation ($\bar{I} = 1$)	Kernel	Free terms from axial differentiation ($\bar{I} = 3$)
$U_{\rho 1,\rho}$	$\frac{(17-20\nu)}{60(1-\nu)G}$	$U_{\rho 3,\rho}$	$\frac{1}{60(1-\nu)G}$
$U_{\zeta 1,\zeta}$	$\frac{-1}{30(1-\nu)G}$	$U_{\zeta 3,\zeta}$	$\frac{7-10\nu}{30(1-\nu)G}$
$U_{\rho 1}$	$\frac{-1}{12(1-\nu)G}$	$U_{\rho 3}$	$\frac{-1}{12(1-\nu)G}$

The method used here for large strain–large rotation problems is very similar to that outlined in Refs [1, 7]. Once the iterative calculations are completed at the end of a time step, the boundary values of v_i, $\dot{\tau}_i$ and $v_{i,j}$ are determined at each boundary node. It is then a simple matter to determine $\dot{t}_i$ through the use of eqns (13).

At this stage, it is convenient to transform $\dot{t}_R$ and $\dot{t}_Z$ into local coordinates normal and tangential to the boundary at a boundary point P. Now, from eqn (8)

$$\mathring{\sigma}_{nn} = \dot{t}_n, \quad \mathring{\sigma}_{nc} = \dot{t}_c \tag{16}$$

where $\mathring{\sigma}_{nn}$ and $\mathring{\sigma}_{nc}$ are the normal and shearing components of the Jaumann rates for the Cauchy stress at P. The rest of the algorithm follows that outlined in Refs [1, 7] with constitutive equations (from eqn (5)) written as

$$\frac{\partial v_c}{\partial c} = d_{cc} = \frac{1}{E}[\mathring{\sigma}_{cc} - \nu(\mathring{\sigma}_{nn} + \mathring{\sigma}_{\theta\theta})] + d_{cc}^{(n)}$$

$$\frac{v_R}{R} = d_{\theta\theta} = \frac{1}{E}[\mathring{\sigma}_{\theta\theta} - \nu(\mathring{\sigma}_{nn} + \mathring{\sigma}_{cc})] + d_{\theta\theta}^{(n)}. \tag{17}$$

These equations are solved for the unknown stress rates $\mathring{\sigma}_{cc}$ and $\mathring{\sigma}_{\theta\theta}$, and then these, together with $\mathring{\sigma}_{nn}$ and $\mathring{\sigma}_{nc}$ are transformed back to global coordinates. Finally, the material rates $\dot{\sigma}_{RR}$, etc. in global coordinates, are obtained from eqns (15). It is noted here that eqn (18) in Ref. [7] should read $\dot{\sigma}_{ZZ} = \dot{\sigma}_{nn} + \dot{\sigma}_{cc} - \dot{\sigma}_{RR}$.

NUMERICAL IMPLEMENTATION

Discretization

The first step, as usual, is to divide the boundary ∂B of an R–Z section of the cylinder into N_s boundary segments and the interior into n_i internal cells. Denoting by $v_i(P_m)$ the components of the velocity at a point P which coincides with node M, a discretized version of the boundary equation, eqn (10), can be written as (ρ, ζ not summed, $j = 1$ and 3)

$$\begin{aligned} C_{ij} v_i(P_M) = {} & \sum_{N_s} \int_{\Delta c_n} [U_{\rho j}\dot{\tau}_\rho + U_{\zeta j}\dot{\tau}_\zeta - T_{\rho j}\dot{u}_\rho - T_{\zeta j}\dot{u}_\zeta]\rho_0 \, \mathrm{d}c_0 \\ & + 2G \sum_{n_i} \int_{\Delta A_N} \Bigg[U_{\rho j,\rho} d_{\rho\rho}^{(n)} + U_{\rho j,\zeta} d_{\rho\zeta}^{(n)} + U_{\zeta j,\rho} d_{\zeta\rho}^{(n)} + U_{\zeta j,\zeta} d_{\zeta\zeta}^{(n)} \\ & + \frac{U_{\rho j} d_{\theta\theta}^{(n)}}{\rho_0} \Bigg] \rho_0 \, \mathrm{d}\rho_0 \, \mathrm{d}\zeta_0 + \sum_{n_i} \int_{\Delta A_n} \Bigg[U_{\rho j,\rho} [\sigma_{\rho\rho} d_{\rho\rho} + \sigma_{\rho\zeta}(d_{\rho\zeta} + \omega_{\rho\zeta}) \\ & + U_{\rho j,\zeta} [\sigma_{\rho\rho} d_{\rho\zeta} + \sigma_{\rho\zeta} d_{\zeta\zeta} + \sigma_{\zeta\zeta}\omega_{\rho\zeta}] + U_{\zeta j,\rho} [-\sigma_{\rho\rho}\omega_{\rho\zeta} + \sigma_{\rho\zeta} d_{\rho\rho} + \sigma_{\zeta\zeta} d_{\rho\zeta}] \\ & + U_{\zeta j,\zeta} [\sigma_{\rho\zeta}(d_{\rho\zeta} - \omega_{\rho\zeta}) + \sigma_{\zeta\zeta} d_{\zeta\zeta}] + \frac{U_{\rho j}\sigma_{\theta\theta} d_{\theta\theta}}{\rho_0} \Bigg] \rho_0 \, \mathrm{d}\rho_0 \, \mathrm{d}\zeta_0. \end{aligned} \tag{18}$$

A similar discretized equation can be written for the velocity gradients $v_{j,i}(p)$ at an internal point p. For future reference, this equation will be called eqn (18′).

Suitable shape functions must now be chosen for the variation of velocity and traction rates along boundary elements and for the variation of $d_{ij}^{(n)}$ and $v_{i,j}$ over internal cells. The last approximation is necessary since the velocity gradients are present in the domain integrals in both eqns (18) and (18′), and the solution must be obtained by an iterative procedure at each time step[2–6]. It should be mentioned here that the velocity gradients are also present in the boundary integrals in eqns (18) and (18′), through eqns (13). Separate boundary shape functions need not be chosen for $v_{i,j}$ on the boundary. Instead, the domain

shape functions for these quantities can be used to approximate $v_{i,j}$ at boundary nodes during the iterative process.

The idea here is to discretize eqns (18) and (18′) to obtain algebraic systems with the traction rates, velocities and velocity gradients as unknowns. The solution for these quantities is obtained at a given time by an iterative procedure. Next, the elastic velocity gradients, the Jaumann rates of the Cauchy stress components, and finally their material rates are determined at this time. The complete solution is finally obtained by a time-marching procedure together with suitable updating of the geometry and the kernels. This procedure has been described several times before in the context of two-dimensional problems[2–6] and will not be repeated here.

Integration of kernels

Of crucial importance in the BEM is the accurate numerical evaluation of the integrals of products of singular kernels and shape functions of the unknowns, over boundary elements as well as internal cells. It is pointed out again that the kernels U_{ij} are ln r singular while T_{ij} are $1/r$ singular over the boundary. Also, first as well as second spatial derivatives of U_{ij}, the latter being $1/r^2$ singular, must be integrated over internal cells. All these kernels contain elliptic functions so that analytical/numerical methods must be developed for this purpose. Also, these elliptic integrals are highly sensitive and great care must be exercised in integrating them.

Special methods have been described in Refs [1, 7] for the integration of the kernels U_{ij} and T_{ij} over boundary elements and for the integration of $U_{ij,k}$ over internal cells. In short, a simple transformation $r = e^2$ is very useful for the first integration while a special mapping technique has been successfully used for the domain integration of kernels like $U_{\rho j,\rho}$. The T_{ij} integrals have been obtained indirectly through the use of a rigid body translation mode in the Z-direction and inflation mode in the R-direction. Domain integration of second derivatives of U_{ij} was avoided in Ref. [7] by using the so-called "strain rate gradient method".

The "strain rate gradient method" is impractical for these large deformation problems since such a method would introduce spatial derivatives of terms like $\sigma_{\rho\rho}d_{\rho\rho}$ in the domain integrals in an equation like eqn (14). Brebbia *et al.*[20] have suggested an elegant method for the integration of $U_{ij,kl}$ over internal cells. This method, however, relies on the separation of the radial and the angular dependence of the $U_{ij,kl}$ kernels. This is possible for two-dimensional but not for axisymmetric problems where complicated elliptic functions of R, Z, ρ and ζ are present in the kernels. A new and accurate method for calculating these integrals, for large deformation axisymmetric problems, is outlined below.

Singular integration of $U_{ij,kl}$ over internal cells

It is easiest to explain this procedure in terms of local polar coordinates (r, ψ) centered at the source point (R, Z) and lying in the R–Z plane. Here r is the distance between the source and the field point and ψ is the angle made by the line pq to the R-axis in the R–Z plane (Fig. 2).

The kernels $U_{\rho 1,\rho 1}$, etc. in eqn (14) contain terms with the strongest singularity $1/r^2$

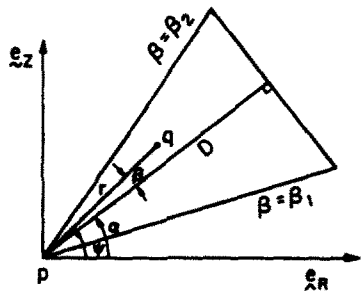

Fig. 2. Notation used for the evaluation of domain integrals.

and the next strongest $1/r$. A typical term containing $U_{\rho 1,\rho 1}$ in eqn (14) can be written as

$$\int_{B^0} U_{\rho 1,\rho 1}(p,q)\,g(q)\,\mathrm{d}A_q = \int_{B^0}\left[U_{\rho 1,\rho 1}(p,q)\,g(q) - \frac{f(\psi)}{r^2}\,g(p)\right]\mathrm{d}A_q + g(p)\int_{B^0}\frac{f(\psi)}{r^2}\,\mathrm{d}A_q \tag{19}$$

where $f(\psi)/r^2$ is the term with the strongest singularity in $U_{\rho 1,\rho 1}$ and $g(q)$ is a term multiplying this kernel. The functions $f(\psi)$, for the various kernels $U_{ij,kl}$, have been obtained by using the symbolic computer package MACSYMA[14] and are listed in Table 3. It should be noted here that $U_{ij,kl}$ when $p \in$ axis of symmetry, can be directly put into the form $f(\psi)/r^2$.

The first domain integral in eqn (19) is now only $1/r$ singular and can be obtained by mapping followed by Gaussian integration as described in Refs [1, 7]. The second integral on a triangular cell, using the notation given in Fig. 2, becomes

$$g(p)\int_{\beta_1}^{\beta_2}\mathrm{d}\psi\int_{\varepsilon}^{D/\cos\beta}\frac{f(\psi)}{r}\,\mathrm{d}r = g(p)\int_{\beta_1}^{\beta_2} f(\beta)\ln\left(D/\cos\beta\right)\mathrm{d}\beta. \tag{20}$$

The value of the integral at the lower limit $\varepsilon \to 0$ vanishes when all contiguous elements around p are taken into account since, due to the nature of the kernels

$$\int_0^{2\pi} f(\psi)\,\mathrm{d}\psi = 0 \quad \text{if} \quad p \notin \text{axis of symmetry}$$

and

$$\int_0^{\pi} f(\psi)\,\mathrm{d}\psi = 0 \quad \text{if} \quad p \in \text{axis of symmetry.}$$

Table 3. Singular functions from $U_{ij,kl}$ ($c_1 = 1/8\pi(1-\nu)G$, $c_2 = (3-4\nu)$)

Kernel	$f(\psi)/c_1$
$U_{\rho 1,\rho 1}$	$(\cos 2\psi - \cos 4\psi - c_2 \cos 2\psi)$
$U_{\rho 1,\zeta 1}$	$-(\sin 4\psi + c_2 \sin 2\psi)$
$U_{\zeta 1,\rho 1}$	$(\sin 2\psi - \sin 4\psi)$
$U_{\zeta 1,\zeta 1}$	$\cos 4\psi$
$U_{\rho 1,\rho 2}$	$-(\sin 4\psi + c_2 \sin 2\psi)$
$U_{\rho 1,\zeta 2}$	$(\cos 2\psi + \cos 4\psi + c_2 \cos 2\psi)$
$U_{\zeta 1,\rho 2}$	$\cos 4\psi$
$U_{\zeta 1,\zeta 2}$	$(\cos 2\psi + \cos 4\psi + c_2 \cos 2\psi)$
$U_{\rho 2,\rho 1}$	$(\sin 2\psi - \sin 4\psi)$
$U_{\rho 2,\zeta 1}$	$\cos 4\psi$
$U_{\zeta 2,\rho 1}$	$(\cos 4\psi - \cos 2\psi - c_2 \cos 2\psi)$
$U_{\zeta 2,\zeta 1}$	$(\sin 4\psi - c_2 \sin 2\psi)$
$U_{\rho 2,\rho 2}$	$\cos 4\psi$
$U_{\rho 2,\zeta 2}$	$(\sin 2\psi + \sin 4\psi)$
$U_{\zeta 2,\rho 2}$	$(\sin 4\psi - c_2 \sin 2\psi)$
$U_{\zeta 2,\zeta 2}$	$-(\cos 2\psi + \cos 4\psi - c_2 \cos 2\psi)$

It should be noted here that the above integral between 0 and π, for the case $p \in$ axis of symmetry, vanishes for the combination $U_{\rho j,\rho 1} + U_{\rho j,1}/\rho$ (rather than for each term separately). Here $d_{\rho\rho} = d_{\theta\theta}$ and $\sigma_{\rho\rho} = \sigma_{\theta\theta}$.

Thus, the integral in eqn (20) is now completely regular and can be evaluated by usual Gaussian quadrature. Of course, the complete integral over the domain B^0 is obtained by summing over triangular cells as usual. Also, the above procedure is only used for accurate evaluation of the singular integrals. If the domain cell is far from a source point, regular Gaussian integration is sufficient. "Nearly singular" cases, where the source point is outside but very near the domain of integration, require special care, usually perhaps the use of more Gauss points in these regions. Such special treatment for "nearly singular" cases has not been necessary in this work.

It should be mentioned here that the above procedure was inspired by the method outlined in Brebbia *et al.*[20] for the evaluation of similar singular integrals in two dimensions. The method described above, however, is completely general and can be applied to very complicated singular kernels and allows the prescription of arbitrary shape functions for the functions $g(q)$. It can be generalized even further by adding and subtracting the $1/r$ singular portions also from $U_{\rho 1,\rho 1} g(q)$. That would then lead to regular integrals which could, in principle, be evaluated directly by Gaussian quadrature without the need for any shape functions for $g(q)$. Shape functions for $g(q)$ have been used in this work since the unknown velocity gradients occur in the "geometric correction" integrals in equations such as eqns (10) and (14).

Checking numerical calculations by inelastic modes

Schemes for numerical evaluation of singular integrals, such as the ones described above, can be checked in elegant fashion through the use of "inelastic modes". To this end, an axisymmetric version of eqn (9), for small strains, but allowing compressible inelastic deformation (i.e. $\varepsilon_{kk}^{(n)} \neq 0$), can be written as ($j = 1$ and 3, no sum over ρ or ζ)

$$u_{j,I} = \int_{\partial B} [U_{\rho j,I}\tau_\rho + U_{\zeta j,I}\tau_\zeta - T_{\rho j,I}u_\rho - T_{\zeta j,I}u_\zeta]\rho \, \mathrm{d}c$$

$$+ 2G\frac{\partial}{\partial x_I}\int_B \left[U_{\rho j,\rho}\varepsilon_{\rho\rho}^{(n)} + U_{\rho j,\zeta}\varepsilon_{\rho\zeta}^{(n)} + U_{\zeta j,\rho}\varepsilon_{\zeta\rho}^{(n)} + U_{\zeta j,\zeta}\varepsilon_{\zeta\zeta}^{(n)} + \frac{U_{\rho j}}{\rho}\varepsilon_{\theta\theta}^{(n)}\right]\rho \, \mathrm{d}\rho \, \mathrm{d}\zeta$$

$$+ \lambda\frac{\partial}{\partial x_I}\int_B \left[U_{\rho j,\rho} + U_{\zeta j,\zeta} + \frac{U_{\rho j}}{\rho}\right][\varepsilon_{\rho\rho}^{(n)} + \varepsilon_{\zeta\zeta}^{(n)} + \varepsilon_{\theta\theta}^{(n)}]\rho \, \mathrm{d}\rho \, \mathrm{d}\zeta. \tag{21}$$

In purely mathematical terms, one can postulate "inelastic modes" where an imposed displacement field gives rise completely to inelastic strains with zero elastic strains. Such solutions, which give no stresses or tractions, must be admissible solutions to eqn (21) and serve as useful checks of the numerical procedure and for the derivation of free terms. For example, one can use

$$u_Z = Z, \quad \varepsilon_{ZZ}^{(n)} = 1$$

with other strains as well as tractions equal to zero. Now, from eqn (21) ($j = 1$ and 3, no sum over ρ or ζ)

$$u_{j,I} = -\int_{\partial B} T_{\zeta j,I}\zeta\rho \, \mathrm{d}c + \frac{\partial}{\partial x_I}\int_B \left\{(\lambda + 2G)U_{\zeta j,\zeta} + \lambda\left[U_{\rho j,\rho} + \frac{U_{\rho j}}{\rho}\right]\right\}\rho \, \mathrm{d}\rho \, \mathrm{d}\zeta \tag{22}$$

with, of course, $u_{3,3} = 1$ and the rest of the displacement derivatives on the left of the above equation being zero. The left-hand side of the above equation can now be compared against the computed value of the right in order to check the accuracy of the numerical calculations. Other non-elastic modes that have proved useful for this purpose are: (1) $u_R = R$, (2)

$u_R = RZ$, (3) $u_Z = R$, (4) $u_R = R^2$, etc. The beauty of this idea is that *any* single valued postulated displacement field is admissible for this purpose.

Two further comments in this regard are useful.

(a) This inelastic mode idea can also be used to compute derivatives of integrals involving $U_{ij,k}$ rather than to merely check the calculations. It is possible to postulate different modes to indirectly obtain all these derivatives except that the quantities

$$\frac{\partial}{\partial x_I}\int_B U_{\rho j,\zeta}\,\mathrm{d}A \quad \text{and} \quad \frac{\partial}{\partial x_I}\int_B U_{\zeta j,\rho}\,\mathrm{d}A$$

cannot be separately calculated since all inelastic modes give $\varepsilon^{(n)}_{\rho\zeta} = \varepsilon^{(n)}_{\zeta\rho}$. Such separation is not necessary for small strain inelasticity problems where only their sum occurs in eqn (21). They must, however, be calculated separately for large deformation problems.

(b) It should be emphasized here that any use of modes—elastic or plastic—such as those discussed above or in Chapter 6 of Ref. [1], are used only *after* the integral equations have been discretized into algebraic systems of equations in terms of matrices and vectors.

NUMERICAL RESULTS

Illustrative constitutive model

It has been mentioned before that the BEM formulation presented in this paper is quite general and any of a large number of elastic–viscoplastic constitutive models can be used here to describe material behavior. The reader is referred to Mukherjee's book[1] for a discussion of such models.

The particular model chosen for the numerical results discussed in this paper is due to Anand[15]. This is a unified elastic–viscoplastic model with a single scalar internal variable s. The model, adapted to the present multi-axial large deformation situation, is described by the equations

$$d^{(n)}_{ij} = \frac{3}{2}\frac{d^{(n)}}{\sigma}s_{ij} \tag{23}$$

where s_{ij} are the components of the deviatoric part of the Cauchy stress and σ is the stress invariant defined as

$$\sigma = \sqrt{((3/2)s_{ij}s_{ij})}.$$

The invariant $d^{(n)}$ is given by

$$d^{(n)} = A\,\mathrm{e}^{-Q/kT}\,(\sigma/s)^{1/m}, \quad \sigma < s \tag{24}$$

together with the evolution equation

$$\dot{s} = h_0(1 - s/s_c)d^{(n)} \tag{25}$$

with

$$s_c = \tilde{s}\left[\frac{d^{(n)}}{A}\,\mathrm{e}^{Q/kT}\right]^n. \tag{26}$$

Here T is the temperature in Kelvin, Q is the activation energy and k is Boltzmann's constant. Also, A, h_0, $\tilde{s}$, m and n are material constants of which m and n are, in general, temperature dependent. The particular parameters used here are representative of Fe–0.05 carbon steel in a temperature range of 1173–1573 K and strain rate range of

1.4×10^{-4}–2.3×10^{-2} s^{-1}. These parameters have been used for all the isothermal (at $T = 1173$ K) simulations reported here. They are[15]

$$A = 10^{11}\ s^{-1}, \quad h_0 = 1329.22\ \text{MPa},$$
$$\bar{s} = 147.6\ \text{MPa}, \quad m = 0.147, \quad n = 0.03$$
$$Q/k = 3.248 \times 10^4\ \text{K}$$

together with the elastic constants (at 1173 K)

$$E = 5.88 \times 10^3\ \text{MPa}, \quad \nu = 0.3.$$

Also, the initial value of s is taken to be 47.11 MPa.

Shape functions

Boundary ∂B is discretized either into straight boundary elements or into curved quadratic elements in this study. The traction rates and velocities are assumed to be piecewise quadratic on the boundary elements. Region B is discretized into triangular cells. Terms multiplying the kernels in the domain integrals in eqn (10), e.g. $d_{\rho\rho}^{(n)}$ or $\sigma_{\rho\rho}d_{\rho\rho} + \sigma_{\rho\zeta}(d_{\rho\zeta} + \omega_{\rho\zeta})$, are assumed to be piecewise linear on the internal cells with the nodes lying on the vertices of the triangles. Tangential derivatives of velocities are obtained carefully on the boundary by differentiating the boundary shape functions and taking account of the curvature (when present) of the boundary elements. Gaussian quadrature for integration of non-singular kernels typically uses 10 Gauss points on a boundary element and 7 Gauss points on an internal cell.

Problems considered

Three problems are considered as numerical examples in this work. These problems, which have simple geometries, are chosen here because it is possible to generate direct solutions in these cases. As is well known, it is very difficult to generate exact solutions for large deformation problems of the type that are considered in this paper. These direct solutions are compared against the BEM solutions in order to test the accuracy of the numerical results. It is important to emphasize here that the BEM computer program that has been generated here is completely general and can be used to solve large strain–large rotation problems for bodies of arbitrary shape, subjected to arbitrary boundary conditions, as long as the geometry and loading are axisymmetric. This general BEM program has been employed to generate the numerical results that are reported in this paper.

The three problems that are considered here are given below.

(1) Uniaxial extension of a rod. Here the normals on straight boundaries do not rotate during deformation. The boundary conditions in this problem are prescribed velocities and traction-free surfaces.

(2) Expansion of a sphere under a time varying pressure loading at the inner surface.

(3) Expansion of a sphere under a constant prescribed velocity at the inner surface.

Problems (2) and (3) have spherical symmetry and it is sufficient to consider a small (here five-degree) section for the BEM model. Also, since linear variation of the domain terms are prescribed here, the load correction terms (equation (13)) must be incorporated even for the cases where the velocities are prescribed at the boundary.

Numerical results for sample problems

The first problem considered here is that of a uniform rod held at one end and pulled with a uniform velocity at the other end. Half of the rod is modelled in this case. It is possible to obtain a direct solution for this problem by stepwise time integration with updating of the geometry.

The meshes for this problem are given in Fig. 3 and the stress–elongation plots of an internal point from a direct and BEM solution are given in Fig. 4. The BEM solution from

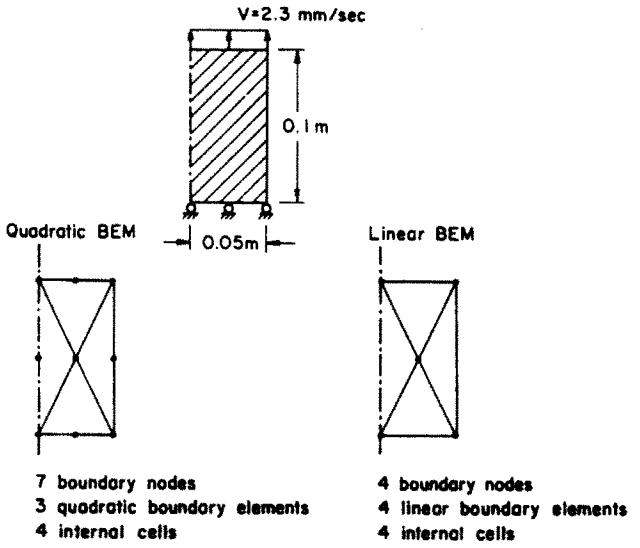

Fig. 3. BEM discretizations for the uniaxial extension problem

the quadratic mesh is seen to agree very well with the direct solution up to a large (40%) amount of strain. In both cases, the BEM predicts stiffer behavior compared to the direct solution.

The next problems considered are those of uniform expansion of a thick spherical shell subjected either to increasing internal pressure or to prescribed radial velocity at the inner surface. Again, the idea is to compare the BEM results with those of a direct solution.

Generating direct solutions for large expansion of a sphere made of a compressible material is not an easy task. However, the corresponding problem for a sphere made of an incompressible material ($\nu = 0.5$) can be solved fairly easily and this solution is briefly outlined in the Appendix. The BEM formulation *presented in this paper* does not admit the incompressible case ($\nu = 0.5$) since the Lamé parameter λ, which occurs in the hypoelastic equation, eqn (5), as well as in Hooke's law for the reference field, blows up in this limit. It is possible to generate an alternative BEM formulation for the incompressible case by suitable modification of the appropriate equations, as is done for compressible linear elasticity. Such has not been done in this work. Instead, in order to validate the present code, a value close to $\nu = 0.5$ has been chosen and the BEM results are compared with

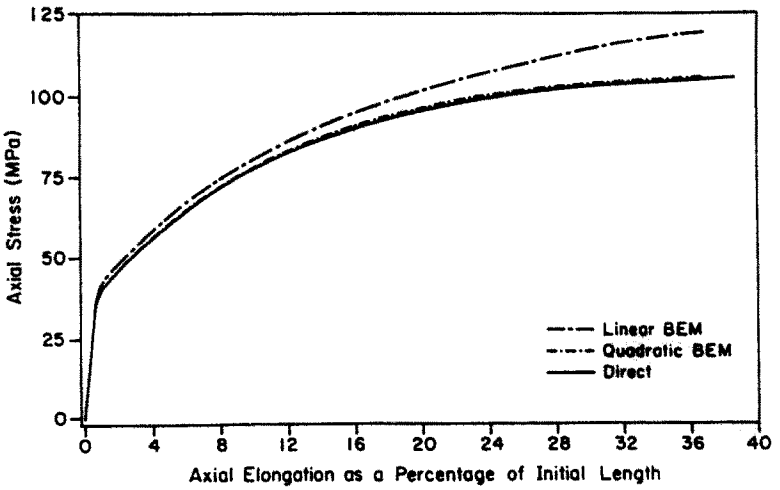

Fig. 4. Stress as a function of elongation for the uniaxial extension problem—comparison of various solutions.

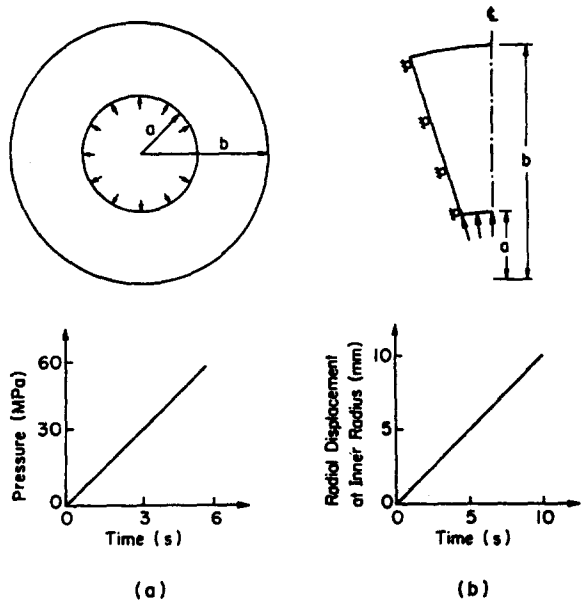

Fig. 5. Inflation of a sphere: (a) prescribed pressure rate at the inner radius; (b) prescribed velocity at the inner radius ($a = 0.1$ m, $b = 0.15$ m, $\dot{p} = 10$ MPa s^{-1}, $v = 1$ mm s^{-1}).

direct solutions for the expansion of a sphere made of an incompressible material. The value of ν, closest to 0.5, which gives stable results from this BEM formulation, is 0.488. This value has therefore been used. Since the direct solution has been verified to be insensitive to the value of ν in the neighborhood of 0.5, this comparison of the BEM and direct results is considered valid and useful.

A five-degree section of a sphere is modelled as shown in Fig. 5 and the BEM mesh for this problem is given in Fig. 6. Only quadratic boundary interpolation is considered here. The numerical results for the prescribed rate of pressure problem are given in Figs 7–9 and the results for the prescribed velocity problem are given in Figs 10–12.

Once again, the agreement between the direct and BEM solutions is quite good, although there are some differences between them at larger strains—especially for the problem with kinematic boundary conditions. It should be emphasized again that the BEM, as formulated in this paper, obtains internal stress rates through exact differentiation (eqns (14)) of the velocity equations. This procedure eliminates jumps in stresses across interelement boundaries—as is typical in the finite element method (FEM)—and greatly contributes to accurate determination of the stresses as well as the non-elastic strains which are driven by the stresses.

Computer times

All problems considered here were run on an IBM 3090/400 and the CPU times are given in Table 4.

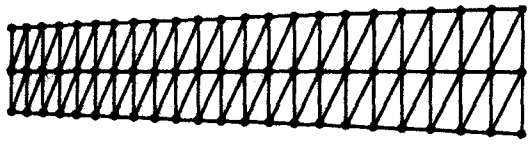

Fig. 6. Boundary element mesh for inflation of a sphere: 27 boundary nodes, 13 quadratic boundary elements, 88 internal cells.

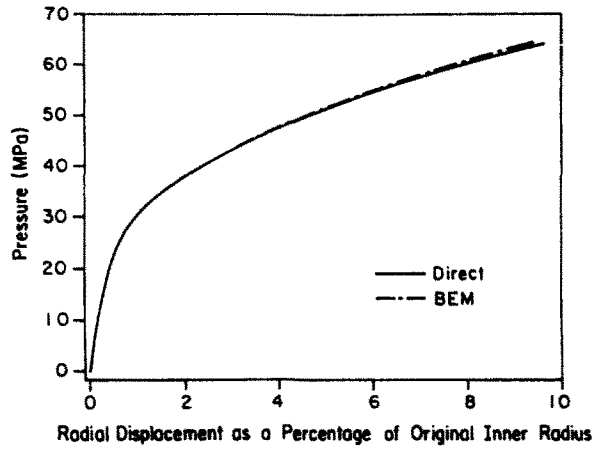

Fig. 7. Pressure as a function of radial displacement of the inside surface of a sphere—$\dot{p}$ prescribed on inside surface.

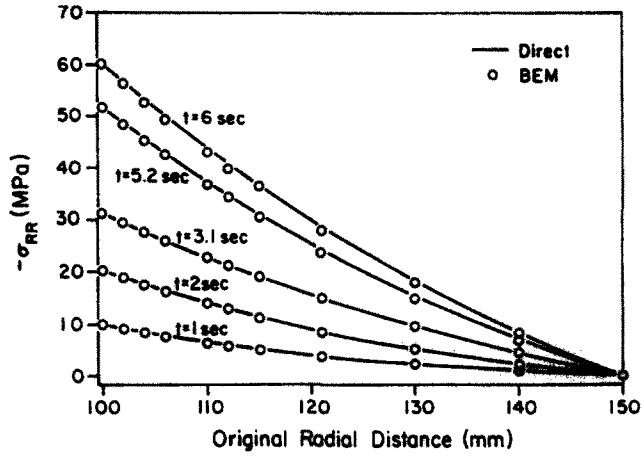

Fig. 8. Same situation as Fig. 7—comparison of BEM and direct solutions for the redistribution of radial stress.

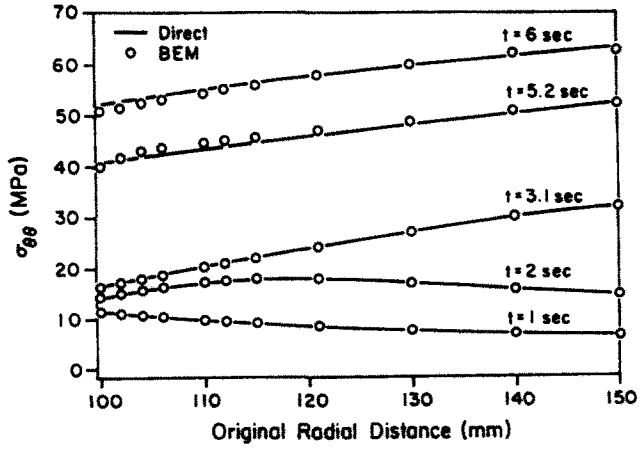

Fig. 9. Same situation as Fig. 7—comparison of BEM and direct solutions for the redistribution of tangential stress.

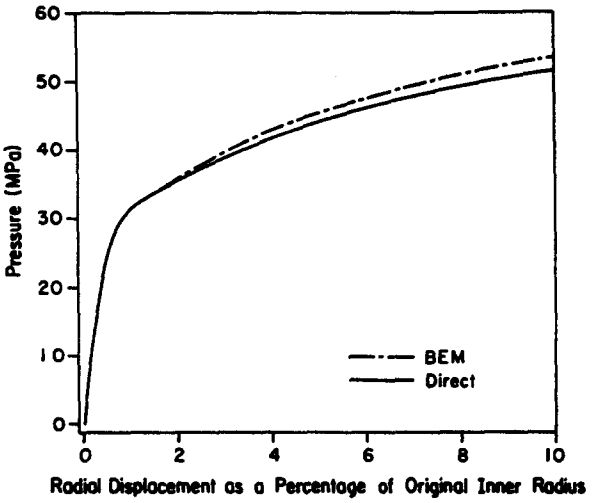

Fig. 10. Pressure as a function of radial displacement at the inside surface of a sphere—v prescribed on the inside surface.

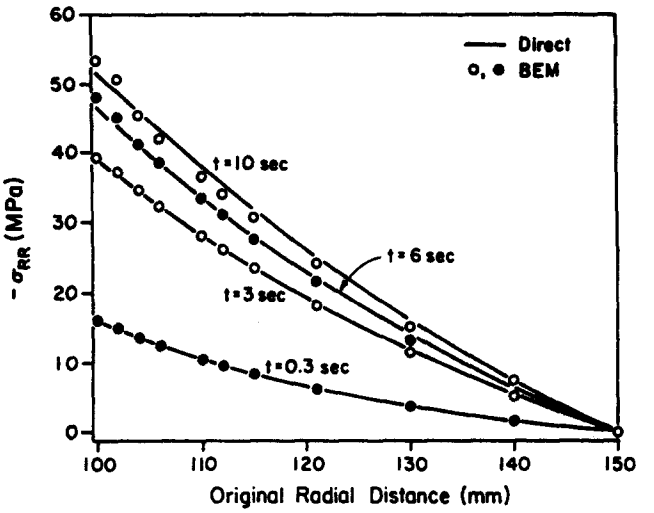

Fig. 11. Same situation as Fig. 10—comparison of BEM and direct solutions for the redistribution of radial stress.

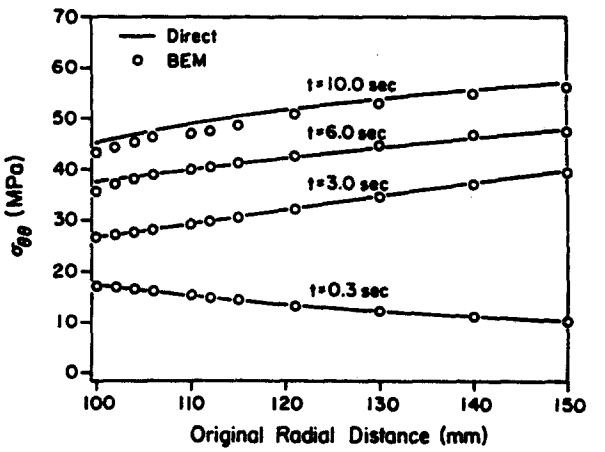

Fig. 12. Same situation as Fig. 10—comparison of BEM and direct solutions for the redistribution of tangential stress.

Table 4. BEM program statistics

Problem	Boundary nodes	Internal nodes	CPU (s)
1. Uniaxial tension :			
linear BEM	4	1	31.1
quadratic BEM	7	2	54.2
2. Inflation of a sphere :			
prescribed pressure rate	27	42	4918.7
prescribed velocity rate	27	42	6214.3

CONCLUSIONS

This paper presents a first attempt at solving axisymmetric boundary value problems, with both geometrical and material nonlinearities, by the boundary element method. The computer program, based on the BEM, has been validated by comparing BEM numerical results against direct solutions for some problems. The numerical results, for simulations into large strain–large rotation regimes, are quite accurate. Further applications of the formulation in the area of metal forming is the subject of continuing research.

One important point deserves special mention in the context of the BEM vs the common method of choice for these problems, the FEM. This point is related to the question of accuracy of stresses and consequently non-elastic strain rates. The stress rates at internal points are obtained here by exact differentiation of the velocity field. This procedure eliminates jumps in stresses across interelement boundaries as is common in the FEM. It is felt that this feature of the BEM greatly contributes to the accurate numerical determination of the stresses as functions of time. This matter is of crucial importance since the stresses drive the solution through time and non-elastic strain rates are typically extremely sensitive functions of the stresses.

It should be mentioned again that the strongly singular and sensitive kernels in the BEM need very careful attention if a BEM implementation for this formidable class of problems is to succeed. Such matters have been given careful consideration in this work.

Acknowledgements—The research reported here has been supported by NSF grant number MSM-8609391 to Cornell University. The computing has been supported by the Production Supercomputer Facility of Cornell University.

REFERENCES

1. S. Mukherjee, *Boundary Element Methods in Creep and Fracture*. Elsevier Applied Science, Barking, Essex, U.K. (1982).
2. A. Chandra and S. Mukherjee, Applications of the boundary element method to large strain–large deformation problems of viscoplasticity. *J. Strain Analysis* **18**, 261 (1983).
3. S. Mukherjee and A. Chandra, Boundary element formulations for large strain–large deformation problems of plasticity and viscoplasticity. In *Developments in Boundary Element Methods*—III (Edited by P. K. Banerjee and S. Mukherjee), p. 27. Elsevier Applied Science, Barking, Essex, U.K. (1984).
4. S. Mukherjee and A. Chandra, Nonlinear solid mechanics. In *Boundary Element Methods in Mechanics* (Edited by D. E. Beskos). North Holland, Amsterdam (1987), in press.
5. A. Chandra and S. Mukherjee, A boundary element formulation for sheet metal forming. *Appl. Math. Modelling* **9**, 175 (1985).
6. S. Mukherjee and A. Chandra, A boundary element analysis of metal extrusion processes. *ASME J. Appl. Mech.* **54**, 335 (1987).
7. V. Sarihan and S. Mukherjee, Axisymmetric viscoplastic deformation by the boundary element method. *Int. J. Solids Structures* **18**, 1113 (1982).
8. T. Kermanidis, A numerical solution for axially symmetric elasticity problems. *Int. J. Solids Structures* **11**, 493 (1975).
9. T. A. Cruse, D. W. Snow and R. B. Wilson, Numerical solutions in axisymmetric elasticity. *Comput. Struct.* **7**, 445 (1977).
10. D. J. Shippy, F. J. Rizzo and R. K. Nigam, A boundary integral equation method for axisymmetric elastic bodies under arbitrary surface loads. In *Innovative Numerical Analysis for the Engineering Sciences* (Edited by R. Shaw *et al.*), p. 423. University of Virginia Press, Charlottesville, Virginia (1980).
11. D. N. Cathie and P. K. Banerjee, Numerical solutions in axisymmetric elastoplasticity. In *Innovative Numerical Analysis for the Applied Engineering Sciences* (Edited by R. Shaw *et al.*), p. 331. University of Virginia Press, Charlottesville, Virginia (1980).

12. J. C. F. Telles, A boundary element formulation for axisymmetric plasticity. *Proceedings of the Fifth International Conference in Boundary Elements*, Hiroshima, Japan, p. 577 (1983).
13. H. D. Bui, Some remarks about the formulation of three-dimensional thermoelastic problems by integral equations. *Int. J. Solids Structures* **14**, 935 (1978).
14. R. H. Rand, *Computer Algebra in Applied Mathematics: an Introduction to MACSYMA*. Pitman, Boston (1984).
15. L. Anand, Constitutive equations for the rate dependent deformation of metals. *ASME J. Engng Mater. Technol.* **104**, 12 (1982).
16. P. K. Banerjee and S. T. Raveendra, Advanced boundary element method analysis of two and three dimensional problems of elasto-plasticity. *Int. J. Numer. Meth. Engng* **23**, 985 (1986).
17. V. Sarihan, Ph.D. Thesis, Department of Theoretical and Applied Mechanics, Cornell University (1982).
18. H. Rajiyah, Ph.D. Thesis, Department of Theoretical and Applied Mechanics, Cornell University (1987).
19. F. J. Rizzo and D. J. Shippy, A formulation and solution procedure for the general nonhomogeneous elastic inclusion problems. *Int. J. Solids Structures* **4**, 1161 (1968).
20. C. A. Brebbia, J. C. F. Telles and L. C. Wroble, *Boundary Element Techniques*. Springer, Berlin (1984).

APPENDIX

Large deformation of a hollow incompressible sphere—direct solution

A spherical coordinate system (r, θ, ϕ) is employed here

$$\nu = 1/2, \quad d_{kk}^{(n)} = 0, \quad d_{\theta\theta} = d_{\phi\phi}$$

and

$$d_{rr} + 2d_{\theta\theta} = \frac{dv_r}{dr} + \frac{2v_r}{r} = 0 \tag{A1}$$

where v_r is the radial velocity.

Solving eqn (A1), one gets

$$v_r = c(t)/r^2$$

with $c(t)$ a time dependent function to be determined later.

Therefore

$$d_{rr} = -\frac{2c(t)}{r^3}, \quad d_{\theta\theta} = \frac{c(t)}{r^3}. \tag{A2}$$

Constitutive equations

$$\begin{aligned} \dot{\sigma}_{rr} &= -\dot{p} + 2G(d_{rr} - d_{rr}^{(n)}) \\ \dot{\sigma}_{\theta\theta} = \dot{\sigma}_{\phi\phi} &= -\dot{p} + 2G(d_{\theta\theta} - d_{\theta\theta}^{(n)}). \end{aligned} \tag{A3}$$

The function $\dot{p}$ is generally a function of r and t.

Equilibrium

$$\frac{d\dot{s}_{rr}}{dr} - \frac{2(\dot{s}_{\theta\theta} - \dot{s}_{rr})}{r} = 0 \tag{A4}$$

where s_{rr} and $s_{\theta\theta}$ are Lagrange stresses.

Now in the absence of rotation

$$\begin{aligned} \dot{s}_{rr} &= \dot{\sigma}_{rr} - d_{rr}\sigma_{rr} \\ \dot{s}_{\theta\theta} &= \dot{\sigma}_{\theta\theta} - d_{\theta\theta}\sigma_{\theta\theta}. \end{aligned} \tag{A5}$$

Substituting eqns (A2), (A3) and (A5) into eqn (A4) and using the relation $(d\sigma_{rr}/dr) - (2(\sigma_{\theta\theta} - \sigma_{rr})/r) = 0$ in the updated Lagrangian frame, one gets

$$\frac{d\dot{p}}{dr} = F(\dot{c}, \sigma, d, r, t)$$

where

$$F(\dot{c}, \sigma, d, r, t) = -\frac{6\dot{c}(t)}{r^4}(\sigma_{rr} - \sigma_{\theta\theta}) - 2G\frac{d(d_{rr}^{(n)})}{dr} - \frac{4G}{r}(d_{rr}^{(n)} - d_{\theta\theta}^{(n)}). \tag{A6}$$

Solution strategy

(1) Find $\dot{c}(t)$ and $\dot{p}$ at the inner and outer radii from boundary conditions.
(2) Find $\dot{p}$ throughout the domain.
(3) Find $\sigma_r(r, t)$ and $\sigma_\theta(r, t)$.
(4) Update $\sigma_r(r, t)$ and $\sigma_\theta(r, t)$ by integrating the corresponding rates.
(5) Find $v_r = \dot{c}(t)/r^2$.
(6) Update the geometry.
(7) Repeat (1)–(6) till desired time.